

Research Paper

# Nanoparticles Formed by Acoustic Destruction of Microbubbles and Their Utilization for Imaging and Effects on Therapy by High Intensity Focused Ultrasound

Nicholas T. Blum,<sup>1</sup> Adem Yildirim,<sup>1</sup> Rajarshi Chattaraj,<sup>2</sup> Andrew P. Goodwin<sup>1</sup>✉

1. Department of Chemical and Biological Engineering, University of Colorado Boulder, Boulder, CO 80303.
2. Department of Mechanical Engineering, University of Colorado Boulder, Boulder, CO 80309.

✉ Corresponding author: andrew.goodwin@colorado.edu.

© Ivyspring International Publisher. This is an open access article distributed under the terms of the Creative Commons Attribution (CC BY-NC) license (<https://creativecommons.org/licenses/by-nc/4.0/>). See <http://ivyspring.com/terms> for full terms and conditions.

Received: 2016.09.09; Accepted: 2016.11.26; Published: 2017.01.15

## Abstract

This work reports that when PEG-lipid-shelled microbubbles with fluorocarbon interior ( $C_4F_{10}$ ,  $C_5F_{12}$ , or  $C_6F_{14}$ ) are subjected to ultrasound pulses, they produce metastable, fluid-filled nanoparticles that can be re-imaged upon administration of HIFU. The nanoparticles produced by destruction of the microbubbles (MBNPs) are of 150 nm average diameter and can be re-imaged for up to an hour after creation for  $C_4F_{10}$ , and for at least one day for  $C_5F_{12}$ . The active species were found to be fluid (gas or liquid) filled nanoparticles rather than lipid debris. The acoustic droplet vaporization threshold of the nanoparticles was found to vary with the vapor pressure of the encapsulated fluorocarbon, and integrated image brightness was found to increase dramatically when the temperature was raised above the normal boiling point of the fluorocarbon. Finally, the vaporization threshold decreases in serum as compared to buffer, and administration of HIFU to the nanoparticles caused breast cancer cells to completely detach from their culture substrate. This work demonstrates a new functionality of microbubbles that could serve as a platform technology for ultrasound-based theranostics.

Key words: microbubbles, ultrasound pulses

## Introduction

This paper reports the instantaneous conversion of microbubbles to soft nanoparticles and their subsequent re-imaging and therapeutic application by high intensity focused ultrasound (HIFU). Ultrasound equipment is found in nearly all hospitals in the US, and ultrasound imaging is highly versatile and possesses few if any side effects. However, ultrasound is limited in its ability to distinguish soft tissues due to small differences in acoustic impedance. Ultrasound contrast agents are often utilized to not only increase backscatter or nonlinear echoes but also to convert acoustic energy for poration-based therapy.<sup>1-6</sup> The most powerful ultrasound contrast agents are microbubbles, due to their high compressibility and

acoustic impedance mismatch compared to the surrounding medium, and their ability to undergo nonlinear size oscillations near their inherent resonance frequencies.<sup>1,7</sup> As a result, microbubbles can be detected using specialized pulse programs such as Cadence Contrast Pulse Sequencing (CPS) or Doppler.<sup>8</sup> The gas cores of the microbubbles are usually stabilized by a surfactant shell or polymer, several formulations of which have been approved by the FDA for vascular imaging.<sup>9-11</sup> Our group and others have shown that these microbubbles can be further modified for further diagnostic utility *in vivo* detection for disease targeting and biosensing.<sup>12-20</sup> An additional application of microbubbles is sensitization

in applications of therapeutic high intensity focused ultrasound (HIFU). Contrast agents such as microbubbles and nanodroplets have been shown to increase efficacy in a variety of *in vitro* and *in vivo* applications including drug delivery, gene transfection, and cancer cell death.<sup>5,21-29</sup>

A major limitation of microbubbles is their inability to leave the bloodstream due to their large size (1-5  $\mu\text{m}$  diameter), which limits their utility to intravascular imaging.<sup>10,30,31</sup> Thus, nanoscale ultrasound contrast agents are sought for extravascular imaging owing to their ability to accumulate in tissue. Because particles of both large size and high compressibility are required to obtain sufficient ultrasound contrast for imaging, nanoscale ultrasound contrast is predicated on the ability of HIFU to provide sufficient energy to vaporize nanodroplets with a volatile core by a nucleation and growth mechanism.<sup>22,23,32-34</sup> We and others have shown this process to occur with droplets, silica nanoparticles, and polymer nanocaps, and the resulting transient bubbles are visible by ultrasound imaging.<sup>35-43</sup> Similarly, if a microbubble could be converted into smaller, nanoscale particles, the resultant particles could then be expanded by HIFU to generate acoustic signal at locations that are impossible to reach with microbubbles. For example, Huynh et al. recently reported the generation of multimodal imaging particles after the destruction of porphyrin microbubbles using ultrasound to generate photoreactive nanoparticles.<sup>44-46</sup> Additionally, Crum and coworkers have reported on nuclei being present after microbubble destruction.<sup>47,48</sup> However, to our knowledge, no one has reported on the ability of microbubble debris itself being able to nucleate and grow in a manner that can then be visualized by ultrasound imaging, nor provided a plausible hypothesis to its mechanism.

In this study, we report the discovery that nanoparticulate products from microbubble destruction (MBNPs) can themselves interact with HIFU to produce transient bubbles for both imaging and therapy. First, the presence of MBNPs was confirmed by both imaging and nanoparticle tracking analysis (NTA), and their formation was correlated to the original composition of the microbubbles. Next, the fate of the MBNPs after formation was probed by a series of acoustic detection experiments, which suggest that the acoustic contrast derives from a nucleation, coalescence, and collapse mechanism. Finally, this MBNP-based phenomenon was not only confirmed in biological media, but the MBNPs were used to detach tumors cells from culture *in vitro*. The reported findings not only improve understanding of the fate of microbubbles after imaging but also

expand the scope of potential acoustic-based theranostic applications for microbubbles.

## Results and Discussion

The overall scheme of the conversion of microbubbles to soft nanoparticles and their subsequent re-imaging is shown in Figure 1A. Common microbubble formulations for ultrasound imaging contain a perfluorocarbon core, utilized for its colloidal stability, and an encapsulating shell composed of lipids and polymers. In this study, the lipid formulation was 9:1 DPPC:DPPA by mole, with 4 mol % DSPE-PEG-5k added to stabilize the bubbles and prevent coalescence.<sup>12,49</sup> When exposed to low pressure acoustic pulses of 0.19 MI at 1.5 MHz (Sequoia Acuson 512, 4V1 transducer), microbubbles show excellent contrast in cadence contrast pulse sequencing (CPS) mode, which specifically highlights the nonlinear echoes generated by microbubbles<sup>8</sup> (note: Mechanical index, or MI, is defined as the peak negative pressure in MPa divided by the square root of the frequency in MHz). Exposing the microbubbles to higher acoustic pressures of 1.1 MI at 1.5 MHz converts them into a mixture of micelles, liposomes, nanobubbles, and nanodroplets, with a corresponding loss in contrast with respect to the background. This contrast was then restored through simultaneous imaging and orthogonal, repeated pulsing by HIFU (Figure 1B). The signal corresponds to that obtained through passive cavitation detection (PCD), which measures the shock waves from acoustic collapse without additional imaging pulses (Figure S1), such as those generated by a conventional ultrasound scanner. As with CPS imaging, PCD found no evidence of cavitation in suspensions containing liposomes and micelles (Figure S2), indicating that the restored contrast does not result from an interaction of the HIFU and conventional ultrasound waves, but rather from the nucleation, growth, and collapse resulting from HIFU itself. Prior to ultrasound imaging, brightfield microscopy images and subsequent analysis (MATLAB, Mathworks, Inc.) revealed that the synthesized microbubbles were of average size 1.67  $\mu\text{m}$  with a mean concentration of  $4.36 \times 10^9$  bubbles  $\text{mL}^{-1}$  (Figure S3, Table S1). Next, a suspension of  $1 \times 10^7$  bubbles  $\text{mL}^{-1}$  labeled with the red dye DiI was subjected to CPS at 1.35 MPa, resulting in a suspension of nanoparticles with average size 164 nm and average concentration of  $1.64 \times 10^9$  bubbles  $\text{mL}^{-1}$  as measured by Nanoparticle Tracking Analysis (NTA) in fluorescence mode (Figure 2A). The presence of fluorescence indicates that the embedded DiI is present in the MBNP suspension as transferred from the microbubbles. TEM confirmed the presence of objects in this size range comparison between the

liposome solution and the destroyed bubble solution (Figure S4).

Next, the internal phase of the initial microbubble suspension was varied to characterize the internal phase of the acoustically active MBNPs. Microbubbles were formulated with PFB ( $T_b^{\circ} = -2.1^{\circ}\text{C}$ ,  $p_{\text{sat}}^{\circ} = 330.3 \text{ kPa}$ ), vaporized perfluoropentane (PFP,  $T_b^{\circ} = 28^{\circ}\text{C}$ ,  $p_{\text{sat}}^{\circ} = 83.99 \text{ kPa}$ ), or vaporized perfluorohexane (PFH,  $56^{\circ}\text{C}$ ,  $p_{\text{sat}}^{\circ} = 29.1 \text{ kPa}$ ). A separate sample was sonicated without fluorocarbon to form liposomes, which possessed a larger average diameter than the destroyed PFB bubbles (Figure 2A). Each formulation was diluted to approximately  $3 \times 10^6$  bubbles  $\text{mL}^{-1}$  and subjected to the same imaging conditions with three different HIFU pulse energies. The resultant acoustic response varied with its saturation vapor pressure, indicating that gaseous bodies were primarily responsible for the generated acoustic contrast. A hypothesis is that once converted the encapsulated PFP and PFH will undergo condensation but the PFB will not. Thus, increasing the HIFU waveform pulse intensity from  $415 \text{ W/cm}^2$  to  $1660 \text{ W/cm}^2$  did not change acoustic response significantly for PFB (Figure 2B). However, PFP's boiling point is slightly greater than room temperature, so increasing the HIFU power caused a significant change in detected signal that matched that of PFB. Thus, some of the HIFU energy is likely required to first induce the vaporization of the liquid back to gas, followed by detection. In addition, the acoustic signal from destroyed PFP microbubbles increased by about 30-fold between  $20^{\circ}\text{C}$  and  $40^{\circ}\text{C}$ . Since  $40^{\circ}\text{C}$  is above the normal boiling point of PFP, this experiment indicates that the phase change from liquid to gas is critical for the re-imaging events (Figure 2C). An even greater HIFU intensity was required to vaporize the PFH MBNPs, indicating that as the saturation pressure of the core component decreases, a greater number of the destroyed microbubbles form nanodroplets as opposed to nanobubbles. This effect would decrease the overall concentration of the resultant "active" MBNPs, as condensed phases require a much greater amount of energy for vaporization. It was found that MBNPs derived from PFP and PFH exhibited enhanced stability as compared to those derived from PFB, but PFP and PFH MBNPs were still less stable than specifically synthesized PFP and PFH nanodroplets (Figure S5). While some stability appears to be imparted by the choice of fluorocarbon, the reduced stability as compared to nanodroplets may be due to partial lipid coverage on the MBNPs. The increased

stability of PFP MBNPs allowed their isolation by centrifugation (Figure S6). To support the hypothesis that these MBNPs are at least partially composed of nanobubbles, this same procedure was conducted for air bubbles; while the bubbles showed detectable signal as compared to liposomes, the poor stability of air bubbles makes quantitative comparison with fluorocarbon bubbles difficult (Figure S7).

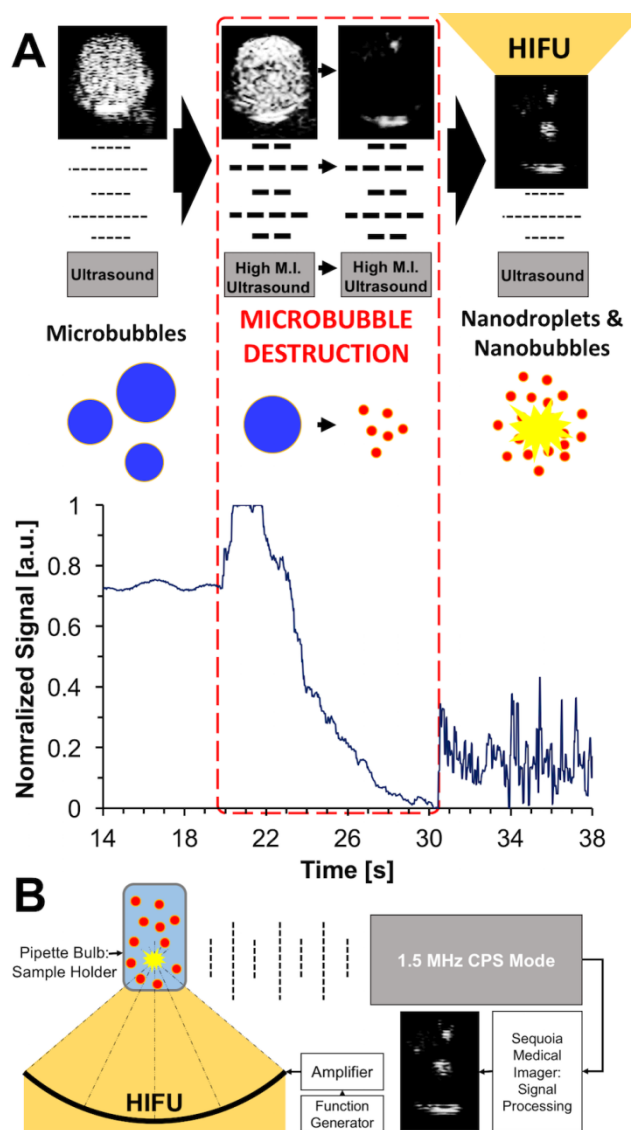


**Figure 1.** (A) Scheme for microbubble destruction and subsequent re-imaging using HIFU and CPS ultrasound. Microbubbles oscillate steadily during low pressure ultrasound pulses which provide a high level of contrast. At 1.35 MPa CPS, represented by the darker dashed lines, the microbubbles are converted into a mixture of nanobubbles and nanodroplets, which can be imaged by applying HIFU. (B) Schematic of the experimental setup. The sample is positioned so that it can be simultaneously exposed to orthogonal pulses of CPS and HIFU to generate contrast from the MBNPs.

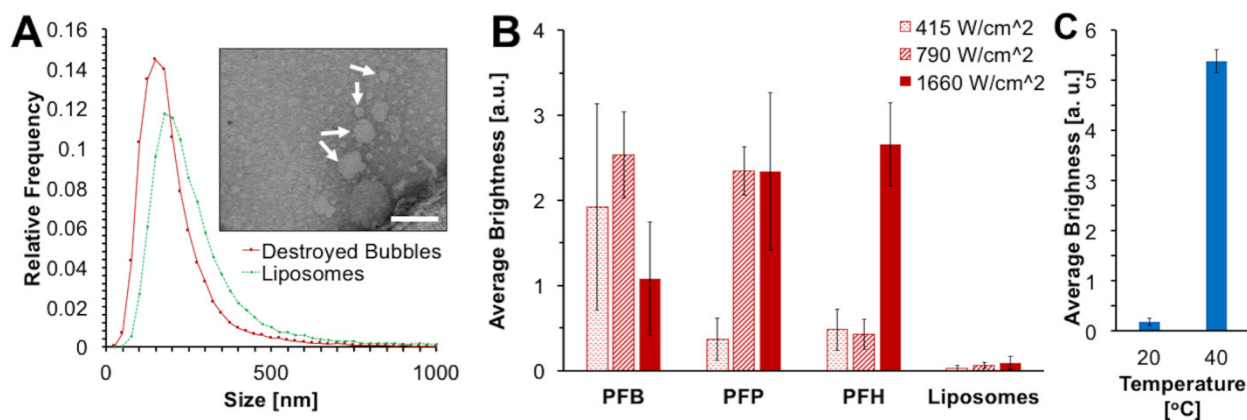


**Figure 2.** (A) Size histogram of CPS-treated PFB MBNPs and liposome suspension as measured by NTA. Inset: representative TEM image of destroyed microbubble suspension with uranyl acetate staining; white arrows indicate examples of MBNP's, and the scale bar is 100 nm. (B) HIFU-induced acoustic response of microbubble suspensions with varying core compositions at 20°C. (C) HIFU-induced acoustic response of destroyed PFP MBNPs suspension at 20°C and 40°C at 415 W/cm<sup>2</sup> HIFU.

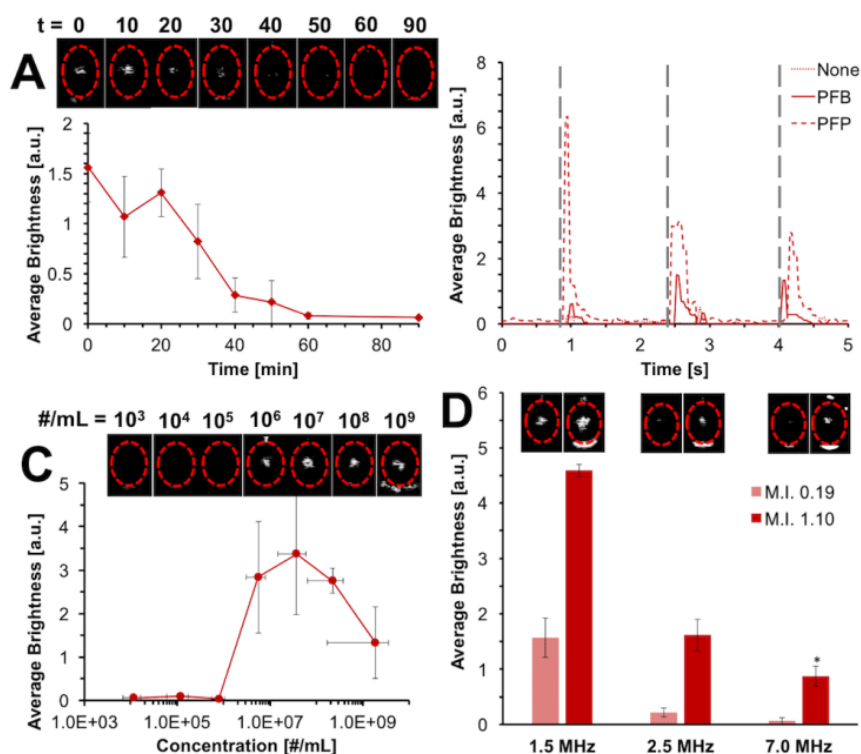


**Figure 3.** (A) HIFU-induced acoustic response of destroyed microbubble solution for varying time after the initial CPS pulse. (B) HIFU-induced acoustic response after single HIFU pulses (gray lines) at 415 W/cm<sup>2</sup>. (C) HIFU-induced acoustic response as function of starting microbubble concentration. Top: representative still images at each concentration. (D) HIFU-induced acoustic response as function of imaging conditions. \* Indicates that imaging was done at 1.90 M.I. instead. All error bars denote one standard deviation from three independent microbubble samples.

We next investigated the acoustic properties of the formed HIFU-active MBNPs. One hypothesis is that HIFU initiates a process of nucleation and fusion with other MBNPs, and together they grow and collapse, generating acoustic energy. Another is that there is a cascade effect where nucleation and/or growth of larger nanobubbles or nanodroplets and their subsequent collapse help provide the energy needed to vaporize the smaller, less responsive liquid nanoparticles. First, MBNPs were generated from a microbubble suspension by CPS, followed by a variable delay time prior to HIFU imaging. In this

experiment, the MBNPs appear to exhibit meta-stability with a half-life of *ca.* 20 min (Figure 3A), which is consistent with a gas body at high Laplace pressure. To check whether the synthesis of these MBNPs were generated during formation of the microbubble solution, the bubbles were stored until several hours after synthesis, then destroyed; the response was consistent regardless of delay time (Figure S8). Next, the HIFU was administered in individual pulses to observe the lifetime of the acoustically-active species (Figure 3B). Each observed signal decayed over a period of *ca.* 500 ms, and the

PCD waveforms (Figure S2) are on the order of *ca.* 70  $\mu$ s, which is consistent with vapor nucleation and growth of a metastable bubble in aqueous media and its subsequent dissolution.<sup>50</sup> Dissolved oxygen and nitrogen did not appear to have an effect on this process (Figure S9), nor did the intensity of the converting CPS pulse (Figure S10). Next, the intensity of detected acoustic signal was found have a strongly nonlinear dependence on the starting microbubble concentration. That is, HIFU-derived acoustic signal from up to  $1 \times 10^6$  microbubbles was almost undetectable, but starting from  $1 \times 10^6$  microbubbles, the signal was close to saturation (Figure 3C). This effect was confirmed by PCD as well (Figure S11). The decrease in signal at high microbubble concentrations may be due to acoustic shadowing of the transducer. The minimum detectable concentration decreased at stronger HIFU acoustic energy (Figure S12), which is consistent with initiation of a pressure-induced phase transition. Finally, the same microbubble destruction and re-imaging process was conducted at different imaging frequencies (Figure 3D). Microbubbles display the greatest contrast at their resonance frequency, and the resonance frequency varies inversely with bubble diameter.<sup>7</sup> Because a Minnaert resonance frequency of 1.5 MHz corresponds to a diameter of  $\sim 4.2 \mu$ m for an unshelled bubble at

ambient conditions, the acoustically active species must be significantly larger than the initial nanobubble.<sup>51</sup> Thus, the HIFU-mediated acoustic mechanism is likely due to a HIFU-induced phase transition that results in rapid bubble growth through nucleation and fusion of neighboring MBNPs, followed by cavitation.

Finally, we sought to determine how the acoustic properties of the formed MBNP's would translate to biomedical applications. First, a microbubble suspension was diluted into fetal bovine serum (FBS) at *ca.* 10 million bubbles  $\text{mL}^{-1}$ , destroyed, and subjected to HIFU at  $415 \text{ W/cm}^2$ . HIFU-induced re-imaging of MBNP's still occurs with no significant quenching of signal in FBS (Figure 4A). Interestingly, the re-imaging threshold of the MBNP's appeared to actually decrease with respect to applied HIFU intensity, initiating at  $200 \text{ W/cm}^2$  as compared to over  $300 \text{ W/cm}^2$  for buffer (Figure 4B). One explanation for this phenomenon is that protein adhesion to the lipid monolayer lowers the barrier to bubble nucleation and growth due to formation of inhomogeneities in the shell. For example, in a separate study in our lab, we found that lateral lipid phase separation reduces the energy barrier to HIFU-induced vaporization of PFH nanodroplets.<sup>52</sup> Another possibility is that surfactant character of serum proteins are stabilizing the growing bubbles as they form. Similar results were obtained for imaging of particles in whole blood (Figure S13).

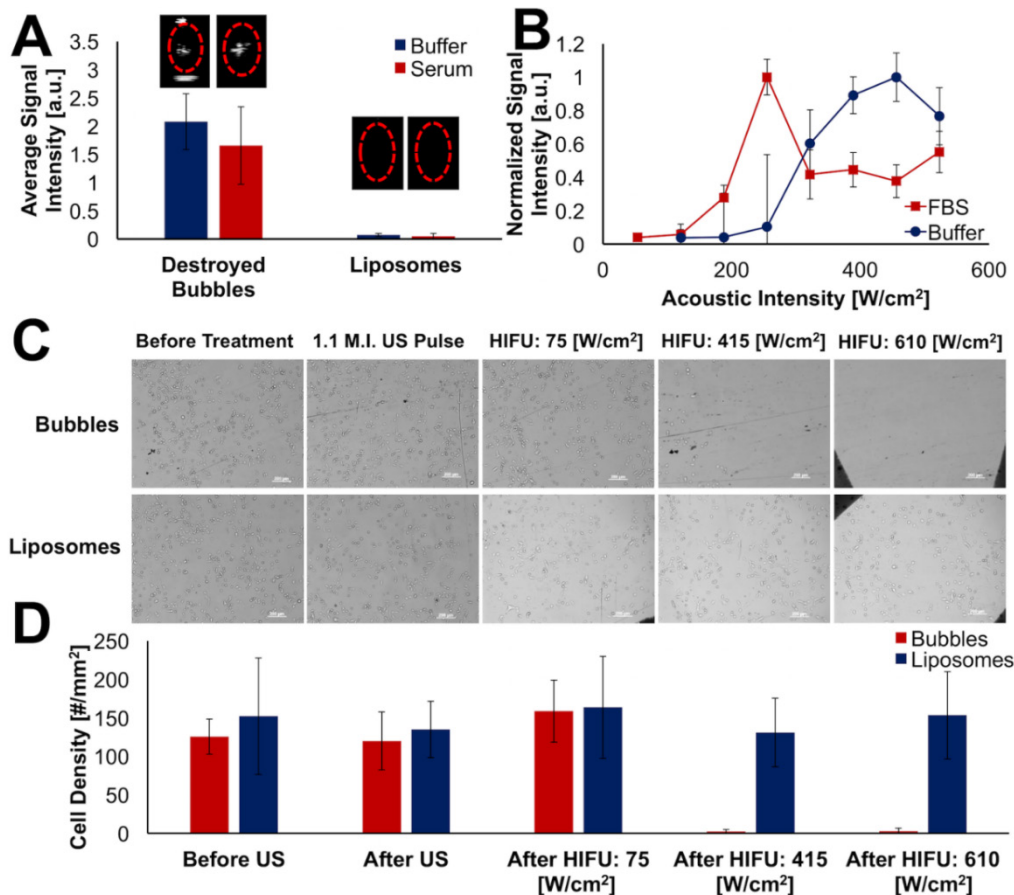


**Figure 4.** (A) Comparison of HIFU-induced acoustic signal of MBNPs to liposomes in TBS and FBS. (B) HIFU-induced acoustic signal of PFB MBNPs as function of starting microbubble concentration in both buffer and FBS. (C) Representative images of MDA-MB-231 cells after specified HIFU treatment. (D) Quantification of the cell density based on bright field images taken. All error bars denote one standard deviation from five replications.

Due to the high energies typically associated with bubble nucleation and collapse, it seemed likely that this imaging modality may produce additional bioeffects similar to those observed upon acoustic stimulation of microbubbles or nanodroplets. In particular, the microjetting caused by bubble collapse can generate shock waves that may result in transient membrane pore formation, production of reactive oxygen species, and/or cell death.<sup>2,3,53,54</sup> To determine if HIFU-sensitized MBNPs could produce similar effects, MDA-MB-231 human breast carcinoma cells were first grown on transparent plastic cell windows (Nunc Opticell). Next, the cells were exposed to CPS ultrasound to create the MBNPs, followed by different intensities of HIFU. After application of HIFU, the breast cancer cells were found to have detached from the culture chamber (Figure 4C). The cell density in the treated area was then quantified (Figure 4D). Tellingly, disruption of cell adhesion only occurred when HIFU intensity was sufficient to initiate nucleation/growth behavior of the MBNPs. To our knowledge, no such observations have been made about this re-imaging phenomenon regarding microbubbles and HIFU.

In conclusion, we have shown that after microbubbles are converted by conventional ultrasound imaging, the resultant particulate suspension can be re-activated through application of high intensity focused ultrasound. The MBNPs are transiently formed, and comparison of different bubble internal phases indicates that the acoustic activity of the MBNP's varies with fluorocarbon vapor pressure. HIFU activity appears to proceed through a nucleation and growth mechanism, with a strong dependence on initial microbubble concentration. Finally, the MBNPs were found to possess enhanced HIFU sensitivity in serum and could cause detachment of cells from their culture environment. Future work will focus on optimizing these MBNPs formulations for theranostic applications such as gene delivery.

## Experimental Methods

**Bubble Formation:** Tris buffered saline (TBS) was prepared to a concentration of 100 mM NaCl (Fisher Scientific) and 10 mM Tris base (Fisher Scientific) and adjusted to a pH of 7.5 with 6 M aqueous HCl (Fisher Scientific). A stock suspension of hydrated 9:1 by mole 1,2-dipalmitoyl-sn-glycero-3-phosphocholine (DPPC):1,2-dipalmitoyl-sn-glycero-3-phosphate (DPPA) (Avanti Polar Lipids, Inc.) was prepared similar to a manner described previously.<sup>13,49</sup> The stock lipid solution was diluted to 1 mg/mL concentration and DSPE-PEG5k (Avanti Polar Lipids, Inc.) was added to a concentration 0.3 mg/mL. The

suspension was then mixed at 75°C for 20 minutes, after which it was cooled to 4°C. This lipid mixture was transferred to a 2 mL centrifuge tube, where the headspace was filled with gaseous PFB by bubbling it through the lipid solution. To form the microbubbles, the probe tip (1/4" diameter) of a probe sonicator (Branson SLPe) was positioned at the liquid gas interface in the tube. The solution was sonicated for 10 s at 70% amplitude while slowly moving the probe tip up as the microbubbles were formed to maintain contact with the interface, a method that we found maximizes yield. PFP bubbles were synthesized in a similar manner, but the PFP (Strem Chemicals) was first evaporated by taking ~0.5 mL in a 10 mL syringe, capping it, and then rapidly expanding the interior volume of the syringe. This same technique was also applied to PFH (Strem Chemicals), which was heated to 55°C immediately prior to sonication. PFP and PFH nanodroplets were synthesized with the same lipid and perfluorocarbon stocks, but using a procedure described in a different report.<sup>55</sup>

**Bubble Fractionation and Sizing:** Bubble fraction and sizing was done in a manner similar to previous communications.<sup>12,49</sup> The bubble suspension was centrifuged at 300 rcf for 3 min, after which the supernatant was removed and replaced with TBS. This wash step was repeated but the bubbles were suspended to a volume of 0.6 mL. This suspension was taken into a 1 mL syringe and allowed to sit for at least 10 min to allow the foam and larger bubbles to float to the top. The bottom 0.5 mL was then transferred to a 4 mL glass vial and the headspace filled with the same gas as in the bubble core. Bubbles were imaged using brightfield images through a 40x objective on an upright Axiomager.A2 microscope (Zeiss). These images were then analyzed by an in-house MATLAB (Mathworks, Inc.) program that identified bubbles using a Hough transform analysis to identify circular objects in the image which allowed for the determination of the size distribution and approximate concentration of the bubble suspension.<sup>12</sup>

**Bubble Ultrasound Imaging and Destruction:** The bubbles were diluted to an approximate concentration of 10 million mL<sup>-1</sup>, unless otherwise specified, and transferred to the tip bulb of a plastic transfer pipette (Fisherbrand). A 4V1 (Siemens Acuson Sequoia) transducer was aligned to acquire horizontal cross-sectional images of the sample within the bulb; this transducer was connected to a Sequoia ultrasound medical imager (Siemens Acuson 512) operating at, unless otherwise specified, 1.5 MHz, in cadence contrast pulse sequencing mode, at an M.I. (mechanical index) of 0.19, and a gain of 18. To destroy the microbubbles, the same imaging

conditions were used but at an M.I. of 1.1, and the sample was imaged at these conditions duration of at least 1 min, or until no bubbles were observable in the sample. At typical experimental concentrations, no bubbles return to the frame when leaving the sample unperturbed, indicating that the signal is not simply due to bubbles diffusing into the frame. To demonstrate activity in degassed solvents, the bubbles were diluted in degassed TBS before destruction. TBS was degassed by stirring at 90°C at reflux for 3 h. Microbubbles can also be destroyed by imaging them continuously at 0.19 M.I. of Sequoia ultrasound for approximately 10 min.

*PCD Setup and Validation:* The passive cavitation detection system was implemented by connecting a 20 MHz single element immersion transducer (Olympus Corp.) to a 5072PR Pulser/Receiver (Olympus Corp.) operating with +40dB gain in receive-only mode. The output was connected via a EF513 6.7 MHz high pass filter (ThorLabs, Inc.) to a Tektronix TDS2012C oscilloscope. The external trigger of the oscilloscope was connected to the previously described function generator. This setup was used in lieu of the Sequoia Acuson 512; the setup was otherwise the same (Figure S1). For each measurement, the data was saved from the oscilloscope and imported to Excel (Microsoft Corp.), where the voltage was squared and then integrated via a left Riemann sum approximation. The resulting value constituted a single measurement; three measurements of three independent samples were combined to give the mean value and standard deviation plotted in the text.

*MBNP Characterization:* The size distribution of MBNPs was determined using fluorescence mode on a Nanosight LM10 setup (Malvern). To make the initial fluorescently labeled MBNPs, first, the DPPC/DPPA stock described above was made with 1 mol% 1,1'-dioctadecyl-3,3',3'-tetramethylindocarbocyanine perchlorate (DiI); the microbubbles were synthesized and destroyed in the usual manner. NTA was measured within 20 min of the microbubble destruction. The TEM images were taken using a CM100 (Phillips) microscope. TEM samples were prepared by first subjecting 100 million bubbles mL<sup>-1</sup> suspension to destruction conditions using Sequoia ultrasound as described above, followed by staining with 2% uranyl acetate for 2 min on a carbon 200 mesh, copper TEM grid (Electron Microscopy Sciences) within 20 min of microbubble destruction. The excess uranyl acetate solution was wicked away, and the remaining film left to air dry. In order to isolate the MBNPs, a PFP bubble solution was diluted 5X and subjected to CPS pulses as described above, then centrifuged for 5 min at 1500 g. Based on the centrifugation equation, this treatment should

sediment 200 nm particles with an internal density of >1300 kg/m<sup>3</sup>. The supernatant was discarded and the pellet was carefully re-suspended to 1 mL by gently pipetting several times.

*MBNP Imaging:* Imaging of the MBNPs via simultaneous HIFU and CPS was performed in a manner similar to previous communications.<sup>35,36,52,55</sup> A High Intensity Focused Ultrasound transducer (Sonic Concepts H101, 64.0 mm Active Diameter × 63.2 mm Radius of Curvature) equipped with a coupling cone (Sonic Concepts C101) was filled with degassed and deionized water, submerged in a water tank, and connected to a 30 MHz Function/Arbitrary Waveform Generator (Agilent Technologies) via an AG Series Amplifier (T&C Power Conversion, Inc.), the latter operating at 100% amplifier output throughout the study. The waveforms were measured, and the peak pressure and acoustic intensities of these HIFU pulses were calculated to be approx. 7.8 MPa via needle hydrophone calibration (Onda Corp.) in free field. The calibration curve corresponding number of applied cycles, or number of continuous waves, to an acoustic intensity can be found in Figure S14. The acoustic intensity is given in W/cm<sup>2</sup> and the intensity for the duration of the pulse. The overall time-averaged acoustic intensity is actually much lower, since there is a pulse generated every 100 ms. Thus, there is about a 0.5% duty cycle.

In a typical experiment, MBNPs in the pipette tip bulb were positioned on top of the coupling cone to ensure proper HIFU focusing into the center of the sample. The appropriate Sequoia transducer, 4V1 for 1.5 and 2.5 MHz imaging and 15L8 for 7 MHz imaging, remained aligned perpendicular to the direction of focus of the ultrasound transducer. HIFU was applied with the following function generator settings: 1 V<sub>pp</sub>, 1.1 MHz center frequency, 0.1 s pulse interval (burst period), and with 6 cycles (sine waves) corresponding to an intensity of 415 W/cm<sup>2</sup> for a single pulse of approximately 6 μs, unless otherwise specified. The recorded videos had a duration of 20 s for each sample. To create the bar graphs of arbitrary units (a.u.), a MATLAB program was used that parsed the videos into a series of images, for each of which the mean pixel brightness of the region of interest (ROI) was determined. The average brightness of each video in the ROI, minus the background, was then taken and plotted. For serum and blood studies, the 1x10<sup>7</sup> bubbles were diluted in fetal bovine serum (HyClone, GE Lifesciences) or bovine whole blood (Lampire, Inc.), respectively, to the desired concentration, destroyed as described above, and then imaged with HIFU. ANOVA, effect, and level tests were conducted for MBNPs and liposomes in TBS, serum, and blood (Figure S15). All statistical analyses

were conducted with JMP Pro 12 (SAS Institute, Inc.).

**Cell Damage Studies:** A MDA-MB-231 breast carcinoma cell line was cultured in sterile DMEM (Fisher Scientific) with 10% serum and 0.5% penicillin. During passaging, approx. 200,000 cells were taken, diluted into 11 mL DMEM, injected into a Nunc Opticell (Nunc Corp.), and allowed to grow for 2 d. The cell media was removed and replaced with 11 mL of cell media containing either 100 million bubbles per mL or an approximately equivalent concentration of 0.1 mg per mL of sonicated lipid solution. The Opticell was then imaged at random spaces using 5x objective. The Opticell was exposed to high mechanical index ultrasound from the Sequoia, followed by random imaging. Finally, 2, 6, or 8 cycles of HIFU were applied to the Opticell at random areas and subsequently imaged using bright field. Cells were counted manually over a fixed area in the acquired images.

## Supplementary Material

Supplementary figures and tables.

<http://www.thno.org/v07p0694s1.pdf>

## Acknowledgements

The authors acknowledge NIH for research support through grants DP2EB020401 and R21EB018034. The authors thank Mr. Jared Snell and Profs. Mark Borden, Tyrone Porter, Ted Randolph, and Jennifer Cha for helpful suggestions. The authors also thank Prof. Stephanie Bryant for use of her cell culture equipment and Dr. Luke Amer for cell culture training.

## Competing Interests

The authors have declared that no competing interest exists.

## References

- Azhari H. *Basics of Biomedical Ultrasound for Engineers*. 1st ed. Hoboken, USA: Wiley-IEEE Press; 2010. doi:10.1002/9780470561478.
- Tran TA, Le Guennec JY, Bougnoux P, Tranquart F, Bouakaz A. Characterization of cell membrane response to ultrasound activated microbubbles. *IEEE Trans Ultrason Ferroelectr Freq Control*. 2008;55(1):44-49. doi:10.1109/TUFFC.2008.615.
- Prentice P, Cuschieri A, Dholakia K, Prausnitz M, Campbell P. Membrane disruption by optically controlled microbubble cavitation. *Nat Phys*. 2005;1:107-110. doi:10.1038/nphys148.
- Deng CX, Sieling F, Pan H, Cui J. Ultrasound-induced cell membrane porosity. *Ultrasound Med Biol*. 2004;30(4):519-526. doi:10.1016/j.ultrasmedbio.2004.01.005.
- Bazan-Peregrino M, Arvanitis CD, Rifai B, Seymour LW, Coussios CC. Ultrasound-induced cavitation enhances the delivery and therapeutic efficacy of an oncolytic virus in an in vitro model. *J Control Release*. 2012;157(2):235-242. doi:10.1016/j.jconrel.2011.09.086.
- Ferrara KW. Driving delivery vehicles with ultrasound. *Adv Drug Deliv Rev*. 2008;60:1097-1102. doi:10.1016/j.addr.2008.03.002.
- Hoff L. *Acoustic Characterization of Contrast Agents for Medical Ultrasound Imaging*. 1st ed. Boston, USA: Kluwer Academic Publishers; 2001. doi:10.1007/9789401706131.
- Phillips PJ. Contrast pulse sequences (CPS): imaging nonlinear microbubbles. 2001 IEEE Ultrason Symp Proceedings An Int Symp (Cat No01CH37263). 2001;2:1739-1745. doi:10.1109/ULTSYM.2001.992057.
- Lindner JR. Microbubbles in medical imaging: current applications and future directions. *Nat Rev Drug Discov*. 2004;3(June):527-532. doi:10.1038/Nrd1417.
- Stride E, Saffari N. Microbubble ultrasound contrast agents: a review. *Proc Inst Mech Eng H*. 2003;217(6):429-447. doi:10.1243/09544110360729072.
- Calliada F, Campani R, Bottinelli O, Bozzini A, Sommaruga MG. Ultrasound contrast agents. *Eur J Radiol*. 1998;27:S157-S160. doi:10.1016/S0720-048X(98)00057-6.
- Nakatsuka MA, Hsu MJ, Esener SC, Cha JN, Goodwin AP. DNA-coated microbubbles with biochemically tunable ultrasound contrast activity. *Adv Mater*. 2011;23(42):4908-4912. doi:10.1002/adma.201102677.
- Nakatsuka MA, Mattrey RF, Esener SC, Cha JN, Goodwin AP. Aptamer-crosslinked microbubbles: smart contrast agents for thrombin-activated ultrasound imaging. *Adv Mater*. 2012;24(45):6010-6016. doi:10.1002/adma.201201484.
- Nakatsuka MA, Barback C V., Fitch KR, et al. In vivo ultrasound visualization of non-occlusive blood clots with thrombin-sensitive contrast agents. *Biomaterials*. 2013;34(37):9559-9565. doi:10.1016/j.biomaterials.2013.08.040.
- Klibanov AL. Targeted delivery of gas-filled microspheres, contrast agents for ultrasound imaging. *Adv Drug Deliv Rev*. 1999;37:139-157. doi:10.1016/S0169-409X(98)00104-5.
- Böhmer MR, Klibanov AL, Tiemann K, Hall CS, Gruell H, Steinbach OC. Ultrasound triggered image-guided drug delivery. *Eur J Radiol*. 2009;70:242-253. doi:10.1016/j.ejrad.2009.01.051.
- Klibanov AL. Ligand-carrying gas-filled microbubbles: Ultrasound contrast agents for targeted molecular imaging. *Bioconjug Chem*. 2005;16:9-17. doi:10.1021/bc049898y.
- Lindner JR. Molecular imaging with contrast ultrasound and targeted microbubbles. *J Nucl Cardiol*. 2004;11(2):215-221. doi:10.1016/j.nuclcard.2004.01.003.
- Tinkov S, Coester C, Serba S, et al. New doxorubicin-loaded phospholipid microbubbles for targeted tumor therapy: In-vivo characterization. *J Control Release*. 2010;148:368-372. doi:10.1016/j.jconrel.2010.09.004.
- Schumann PA, Christiansen JP, Quigley RM, et al. Targeted-microbubble binding selectively to GPIIb/IIIa receptors of platelet thrombi. *Invest Radiol*. 2002;37(11):587-593. doi:10.1097/01.rli.0000031077.17751.b2.
- Dayton PA, Zhao S, Bloch SH, et al. Application of ultrasound to selectively localize nanodroplets for targeted imaging and therapy. *Mol Imaging*. 2006;5(3):160-174. doi:10.2310/7290.2006.00019.
- Zhang P, Porter T. An in vitro study of a phase-shift nanoemulsion: A potential nucleation agent for bubble-enhanced HIFU tumor ablation. *Ultrasound Med Biol*. 2010;36(11):1856-1866. doi:10.1016/j.ultrasmedbio.2010.07.001.
- Lin CY, Pitt WG. Acoustic droplet vaporization in biology and medicine. *Biomater Res Int*. 2013. doi:10.1155/2013/404361.
- Coluccia D, Fandino J, Schwyzer L, et al. First noninvasive thermal ablation of a brain tumor with MR-guided focused ultrasound. *J Ther ultrasound*. 2014;2:17. doi:10.1186/2050-5736-2-17.
- Chan AH, Fujimoto VY, Moore DE, Martin RW, Vaezy S. An image-guided high intensity focused ultrasound device for uterine fibroids treatment. *Med Phys*. 2002;29(11):2611-2620. doi:10.1118/1.1513990.
- Kim HC, Al-Mahrouki A, Gorjizadeh A, Karshafian R, Czarnota GJ. Effects of biophysical parameters in enhancing radiation responses of prostate tumors with ultrasound-stimulated microbubbles. *Ultrasound Med Biol*. 2013;39(8):1376-1387. doi:10.1016/j.ultrasmedbio.2013.01.012.
- Al-Bataineh O, Jenne J, Huber P. Clinical and future applications of high intensity focused ultrasound in cancer. *Cancer Treat Rev*. 2012;38(5):346-353. doi:10.1016/j.ctrv.2011.08.004.
- Luo W, Zhou X, Tian X, et al. Enhancement of ultrasound contrast agent in high-intensity focused ultrasound ablation. *Adv Ther*. 2006;23(6):861-868. doi:10.1007/BF02850207.
- Wang CH, Kang ST, Lee YH, Luo YL, Huang YF, Yeh CK. Aptamer-conjugated and drug-loaded acoustic droplets for ultrasound theranosis. *Biomaterials*. 2012;33(6):1939-1947. doi:10.1016/j.biomaterials.2011.11.036.
- Ferrara K, Pollard R, Borden M. Ultrasound Microbubble Contrast Agents: Fundamentals and Application to Gene and Drug Delivery. *Annu Rev Biomed Eng*. 2007;9(1):415-447. doi:10.1146/annurev.bioeng.8.061505.095852.
- Sboros V. Response of contrast agents to ultrasound. *Adv Drug Deliv Rev*. 2008;60(10):1117-1136. doi:10.1016/j.addr.2008.03.011.
- Reznik N, Williams R, Burns PN. Investigation of Vaporized Submicron Perfluorocarbon Droplets as an Ultrasound Contrast Agent. *Ultrasound Med Biol*. 2011;37(8):1271-1279. doi:10.1016/j.ultrasmedbio.2011.05.001.
- Shpak O, Verweij M, Vos HJ, de Jong N, Lohse D, Versluis M. Acoustic droplet vaporization is initiated by superharmonic focusing. *Proc Natl Acad Sci U S A*. 2014;111(5):1697-1702. doi:10.1073/pnas.1312171111.
- Sheeran PS, Luois S, Dayton P a., Matsunaga TO. Formulation and acoustic studies of a new phase-shift agent for diagnostic and therapeutic ultrasound. *Langmuir*. 2011;27(17):10412-10420. doi:10.1021/la2013705.
- Yildirim A, Chattaraj R, Blum NT, Goldscheiter GM, Goodwin AP. Stable Encapsulation of Air in Mesoporous Silica Nanoparticles: Fluorocarbon-Free Nanoscale Ultrasound Contrast Agents. *Adv Health Mater*. 2016;5(11):1290-1298. doi:10.1002/adhm.201600030.
- Yildirim A, Chattaraj R, Blum NT, Goodwin AP. Understanding Acoustic Cavitation Initiation by Porous Nanoparticles: Toward Nanoscale Agents for

- Ultrasound Imaging and Therapy. *Chem Mater.* 2016;28(16):5962-5972. doi:10.1021/acs.chemmater.6b02634.
37. Kwan JJ, Myers R, Coviello CM, et al. Ultrasound-Propelled Nanocups for Drug Delivery. *Small.* 2015;11(39):5305-5314. doi:10.1002/smll.201501322.
  38. Chen Y, Gao Y, Chen H, et al. Engineering Inorganic Nanoemulsions/Nanoliposomes by Fluoride-Silica Chemistry for Efficient Delivery/Co-Delivery of Hydrophobic Agents. *Adv Funct Mater.* 2012;22(8):1586-1597. doi:10.1002/adfm.201102052.
  39. Liberman A, Wu Z, Barback C V., et al. Color doppler ultrasound and gamma imaging of intratumorally injected 500 nm iron-silica nanoshells. *ACS Nano.* 2013;7(7):6367-6377. doi:10.1021/nn402507d.
  40. Zhao Y, Zhu Y. Synergistic cytotoxicity of low-energy ultrasound and innovative mesoporous silica-based sensitive nanoagents. *J Mater Sci.* 2014;49(10):3665-3673. doi:10.1007/s10853-014-8073-y.
  41. Kempen PJ, Greasley S, Parker KA, et al. Theranostic Mesoporous Silica Nanoparticles Biodegrade after Pro-Survival Drug Delivery and Ultrasound/Magnetic Resonance Imaging of Stem Cells. *Theranostics.* 2015;5(6):631-642. doi:10.7150/thno.11389.
  42. Hu H, Zhou H, Du J, et al. Biocompatible hollow silica microspheres as novel ultrasound contrast agents for in vivo imaging. *J Mater Chem.* 2011;21(18):6576-6583. doi:10.1039/c0jm03915b.
  43. Chiriacò F, Conversano F, Soloperto G, et al. Epithelial cell biocompatibility of silica nanospheres for contrast-enhanced ultrasound molecular imaging. *J Nanoparticle Res.* 2013;15(7):1779. doi:10.1007/s11051-013-1779-y.
  44. Huynh E, Leung BYC, Helfield BL, et al. In situ conversion of porphyrin microbubbles to nanoparticles for multimodality imaging. *Nat Nanotechnol.* 2015;10(4):325-332. doi:10.1038/nnano.2015.25.
  45. Huynh E, Jin CS, Wilson BC, Zheng G. Aggregate enhanced trimodal porphyrin shell microbubbles for ultrasound, photoacoustic, and fluorescence imaging. *Bioconjug Chem.* 2014;25(4):796-801. doi:10.1021/bc5000725.
  46. Huynh E, Lovell JF, Helfield BL, et al. Porphyrin Shell Microbubbles with Intrinsic Ultrasound and Photoacoustic Properties. *J Am Chem Soc.* 2012;134:16464-16467. doi:10.1021/ja305988f.
  47. Chen WS, Matula TJ, Crum LA. The disappearance of ultrasound contrast bubbles: Observations of bubble dissolution and cavitation nucleation. *Ultrasound Med Biol.* 2002;28(6):793-803. doi:10.1016/S0301-5629(02)00517-3.
  48. Brayman AA, Chen W, Matula TJ, Crum LA, Miller MW. The pulse duration dependence of inertial cavitation dose and hemolysis. *IEEE Ultrason Symp.* 2002:1387-1390.
  49. Nakatsuka MA, Lee JH, Nakayama E, et al. Facile One-Pot Synthesis of Polymer-Phospholipid Composite Microbubbles with Enhanced Drug Loading Capacity for Ultrasound-Triggered Therapy. *Soft Matter.* 2011;7:1656-1659. doi:10.1039/C0SM01131B.
  50. Arora M, Ohl CD, Mørch KA. Cavitation inception on microparticles: A self-propelled particle accelerator. *Phys Rev Lett.* 2004;92(17):174501-174504. doi:10.1103/PhysRevLett.92.174501.
  51. Church CC. The effects of an elastic solid surface layer on the radial pulsations of gas bubbles. *J Acoust Soc Am.* 1995;97(3):1510-1521.
  52. Chattaraj R, Goldscheitter GM, Yildirim A, Goodwin AP. Phase behavior of mixed lipid monolayers in perfluorocarbon nanoemulsions and its effect on acoustic contrast. *RSC Adv.* 2016;6:111318-111325. doi:10.1039/C6RA20328K.
  53. O'Brien WD. Ultrasound-biophysics mechanisms. *Prog Biophys Mol Biol.* 2007;93(1-3):212-255. doi:10.1016/j.pbiomolbio.2006.07.010.
  54. Miller DL, Averkiou MA, Brayman AA, et al. Bioeffects Considerations for Diagnostic Ultrasound Contrast Agents. *J Ultrasound Med.* 2008;27(4):611-632. <http://www.jultrasoundmed.org/content/27/4/611.abstract>.
  55. Chattaraj R, Mohan P, Besmer JD, Goodwin AP. Selective Vaporization of Superheated Nanodroplets for Rapid, Sensitive, Acoustic Biosensing. *Adv Healthc Mater.* 2015;4(12):1790-1795. doi:10.1002/adhm.201500315.